

# Sliding Wear Behavior of Al<sub>2</sub>O<sub>3</sub>–TiO<sub>2</sub> Coatings Fabricated by the Suspension Plasma Spraying Technique

E. Klyatskina<sup>1</sup> · L. Espinosa-Fernández<sup>1</sup> · G. Darut<sup>2</sup> · F. Segovia<sup>1</sup> · M. D. Salvador<sup>1</sup> · G. Montavon<sup>2</sup> · H. Agorges<sup>3</sup>

Received: 20 December 2014 / Accepted: 8 April 2015 / Published online: 22 May 2015  
© Springer Science+Business Media New York 2015

**Abstract** The friction and dry sliding wear behavior of alumina and alumina–titania near-nanometric coatings were examined. Coatings were obtained by the suspension plasma spraying technique. Dry sliding wear tests were performed on a ball-on-disk tribometer, with an Al<sub>2</sub>O<sub>3</sub> ball as counterpart material, a normal load of 2 N, a sliding distance of 1200 m and a sliding speed of 0.1 m/s. The effect of including TiO<sub>2</sub> in the fabricated coatings on friction coefficient behavior, wear rates and wear damage patterns was determined. The addition of TiO<sub>2</sub> to the coatings was found to greatly increase wear resistance by, for example, 2.6-fold for 40 wt% of TiO<sub>2</sub>. The analysis of the wear surface was correlated with microstructural parameters, mechanical properties and wear rates.

**Keywords** Al<sub>2</sub>O<sub>3</sub>–TiO<sub>2</sub> · Nanostructured coating · Sliding wear · Suspension plasma spraying

## 1 Introduction

Conventional Al<sub>2</sub>O<sub>3</sub>–TiO<sub>2</sub> coatings are commonly used in machine parts to improve resistance to wear, corrosion, oxidation, erosion and heat [1–3]. Nanostructured Al<sub>2</sub>O<sub>3</sub>–TiO<sub>2</sub> coatings can enhance mechanical properties, such as crack resistance, adhesion strength, spallation resistance and wear resistance [4], which would benefit the shipping, textile, machinery and printing industries [5–7]. However, although many research groups are currently focusing on reducing the size of the particles constituting the coating material [4, 6–12], several limitations still remain in the manufacturing process of nanostructure coatings directly from nano-powders, such as low fluidity and tendency to powder agglomeration, high reactivity and growth rates of nano-particles.

Different processes can be used to produce nanostructure coatings, including atmospheric plasma spraying (APS), high-velocity oxygen fuel spraying and flame or cold-gas spraying [13]. However, suspension plasma spraying (SPS) is one of the more widely used processes to produce finely structured coatings while still maintaining the versatility and flexibility of the thermal spray routes [14]. SPS allows the direct injection of sub-micrometer to nanometer-sized particles into the coating through the use of a liquid as a carrier medium for the suspension particles.

Numerous investigations have been conducted to determine the friction and wear behavior of conventional APS coatings to which TiO<sub>2</sub>, ZrO<sub>2</sub> and/or Cr<sub>2</sub>O<sub>3</sub> have been added [15–20]. Wang et al. [3] reported that dry sliding wear resistance in mild steel coated by APS with nanostructure Al<sub>2</sub>O<sub>3</sub>–13TiO<sub>2</sub> exhibited a fourfold greater wear resistance than samples coated with conventional powder. Fervel et al. [19] found that dry sliding wear resistance was higher in coatings with Al<sub>2</sub>O<sub>3</sub>–40TiO<sub>2</sub> than in those with

✉ E. Klyatskina  
elkl1@upvnet.upv.es

<sup>1</sup> Instituto de Tecnología de Materiales (ITM), Universidad Politécnica de Valencia, Camino de Vera, s/n, 46022 Valencia, Spain

<sup>2</sup> LERMPS-EA3316, Université de Technologie de Belfort-Montbéliard, Site de Sévenas, 90010 Belfort Cedex, France

<sup>3</sup> SPCTS-UMR, CNRS 6638, Faculty of Sciences and Technologies, University of Limoges, 123 Avenue Albert Thomas, 87060 Limoges Cedex, France

$\text{Al}_2\text{O}_3$ – $13\text{TiO}_2$ . Vargas et al. [20] investigated  $\text{Al}_2\text{O}_3$ – $13\text{TiO}_2$  and  $\text{Al}_2\text{O}_3$ – $43\text{TiO}_2$  coatings obtained by APS and concluded that wear resistance was more strongly influenced by hardness than by toughness. Sathish et al. [8] evaluated the dry sliding wear of  $\text{Al}_2\text{O}_3$ – $13\text{TiO}_2$  coatings obtained by APS from a nanopowder and detected an excellent wear resistance which could be attributed to a lower porosity and higher adhesion strength.

To date, however, there have been no attempts to study the wear resistance of coatings obtained by SPS. It is therefore necessary to elucidate the influence of some aspects of the SPS process, such as the reduction of particle size and different levels of  $\text{TiO}_2$  in the coatings, on wear resistance. We report here our investigation on the tribological responses of alumina and alumina–titania near-nanometric coatings obtained by SPS. We found that differences in friction and sliding wear behavior are associated with microstructural and mechanical parameters.

## 2 Experimental Procedure

### 2.1 Materials

Two commercial nanometric powders were used to prepare the coating deposition suspension: AKP30  $\alpha$ - $\text{Al}_2\text{O}_3$  (Sumitomo Chemical Corp., Tokyo, Japan) and K2300  $\text{TiO}_2$  rutile (Kronos, Leverkusen, Germany). Suspensions with an ethanol-base and different compositions of  $\text{TiO}_2$  powder were fabricated under ultrasonic and magnetic stirring. The composition and mass percentages of each coating are given in Table 1.

A carbon steel disc (AISI 1038) with a 50-mm diameter was used as a substrate in the coating deposition. Prior to the spraying process, substrate samples were polished down to 0.07  $\mu\text{m}$  with SiC papers and diamond slurries and then cleaned with ethanol. Substrate samples were then

pre-heated to an average surface temperature of 250  $^\circ\text{C}$  for 40 s to enhance adhesion of the coating.

### 2.2 Coating Deposition

Coating deposition was performed by the SPS technique, using a MultiCoat Plasma platform and Sulzer Metco F4-MB plasma gun (Sulzer, Winterthur, Switzerland), a 6-mm-internal-diameter anode and a mechanical injector specifically built for the suspension by the Science of Ceramic Processing and Surface Treatments (CPCTS) (Université de Limoges, France). Nanometric powder suspensions were injected with a 150- $\mu\text{m}$ -internal-diameter injector through the plasma flow. Suspension momentum density was controlled by adjusting the pressure in the suspension containers upon penetration within the plasma flow. Plasma mass enthalpy remained at the same level for all coating processes. Plasma spraying process parameters used for coating deposition are given in Table 2.

### 2.3 Characterization

Crystalline phase composition of nanoparticles in powders was tested by X-ray diffraction (XRD). Diffractograms were obtained using a Bruker Theta model D8 Advance diffractometer with  $\text{CuK}\alpha$  radiation ( $\lambda = 0.154056 \text{ nm}$ ) (Daltonik GmbH, Bremen, Germany). The generator settings were 40 kV and 30 mA. The XRD data were collected by a diffractometer with Bragg–Brentano ( $\theta/\theta$ ) geometry, in a  $2\theta$  range of  $20^\circ$ – $90^\circ$  with a step width of  $0.015^\circ$  and a counting time of 2 s/step. A PSD (VANTEK; Bruker Daltonik GmbH) solid state detector was used.

Powder morphology and coating fractures were observed by field emission scanning electron microscopy (FESEM; model 7400F; JEOL Ltd., Tokyo, Japan). Coating microstructure was observed in cross-sectioned samples by SEM (model SM6300; JEOL Ltd.) connected to an energy dispersive X-ray (EDX) microanalysis instrument.

**Table 1** Characteristics of the nanometric powder suspensions

Properties	AT coatings <sup>a</sup>							
	AT		AT13		AT25		AT40	
Powder type	$\text{Al}_2\text{O}_3$	$\text{TiO}_2$	$\text{Al}_2\text{O}_3$	$\text{TiO}_2$	$\text{Al}_2\text{O}_3$	$\text{TiO}_2$	$\text{Al}_2\text{O}_3$	$\text{TiO}_2$
Material/powder (wt%)	100	–	87	13	75	25	60	40
$D_{50}$ (nm) <sup>b</sup>	300							
Liquid phase	Et-OH (99.5 %)							
Powder/suspension (wt%)	10							
Dispersant/powder (wt%)	2.0							

<sup>a</sup> AT refers to alumina (A)–titania (T) ( $\text{Al}_2\text{O}_3$ – $\text{TiO}_2$ ), and the number refers to the weight percentage (wt%) of  $\text{TiO}_2$  in the coating

<sup>b</sup>  $D_{50}$  is the median diameter or the medium value of the particle size distribution

**Table 2** Parameters of the plasma spraying process

Parameters	Values
Primary plasma gas flow rate (SLPM)	40 (Ar)
Secondary plasma gas flow rate (SLPM)	20 (He)
Arc current intensity (A)	600
Torch scan velocity (m/s)	1
Scanning step (mm/pass)	10
Spray distance (mm)	30
Spraying time (min)	2

SLPM Standard liters per minute

Coating void contents in samples were not determined due to a lack of adequate protocols [21]. Surface roughness measurements,  $R_a$ , of the coating produced were also obtained with a Perthometer M2 profilometer (Mahr GmbH, Göttingen, Germany).

#### 2.4 Sliding Wear Test

Tribological tests were carried out under dry sliding conditions on a pin-on-disc tribometer (ball-on-disc configuration) manufactured by CSM Instruments (Lausanne, Switzerland), according to ASTM wear testing standards G99-03 [22]. All tests were conducted in a dried mode, and wear debris was continuously removed from the wear track by compressed air. The counter material was a ball of  $\alpha$ - $\text{Al}_2\text{O}_3$  (radius 6 mm, hardness 2400  $\text{HV}_{10}$ ) produced by GMS Ball Co Ltd. (West Sussex, UK). The parameters of the tests were: a contact load of 2 N, sliding speed of 0.1 m/s, sliding distance of 1200 m and a wear track radius of 12.5 mm. Standardized environmental conditions were maintained in all tests:  $23 \pm 2$  °C and  $60 \pm 2$  % relative humidity. In order to obtain sufficient representative values of each investigated parameter, we performed a series of three tests for each material. The surface of each sample was polished to an  $R_a$  of  $<1$   $\mu\text{m}$  to achieve a uniform surface condition and cleaned before the wear test. Wear tracks and cross-sections of the wear surfaces were examined by SEM (model SM6300; JEOL Ltd.) and EDX.

Wear volume loss,  $V_{\text{wear}}$ , was determined from the wear track profile. Track profiles were measured using a Taylor–Hobson surface profiler (Leicester, UK) equipped with a diamond tip of radius 5  $\mu\text{m}$ . Ten random measurements were obtained from each wear track and averaged after an adjustment of 20 %, i.e. the highest and the lowest values were discarded. The wear rate,  $K_v$ , was calculated according to the wear formula of Lancaster [23], as shown in Eq. (1)

$$K_v = \frac{V_{\text{wear}}}{F_N \times S} [\text{mm}^3 \text{N}^{-1} \text{m}^{-1}] \quad (1)$$

where  $V_{\text{wear}}$  is the volume lost expressed in cubic millimeters ( $\text{mm}^3$ ),  $F_N$  is the normal load applied in newtons (N) and  $S$  is the sliding distance in meters (m).

## 3 Results and Discussion

### 3.1 Coating Architecture

The SEM micrographs of cross-sections of the alumina and alumina–titania coatings produced by SPS are shown in Fig. 1. No clear evidence of the real microstructure of the SPS samples was found, possibly due to: (1) the coatings presenting a finer microstructure; (2) limited resolution of the SEM; (3) contamination during the metallographic step due to the appearance of voids from particles which were removed and re-introduced to the surface during the polishing process. Therefore, SEM micrographs of SPS coating samples were only used to estimate coating thickness, as shown in Table 3.

Surface roughness measurements of the different coatings produced,  $R_a$  initial, is also shown in Table 3. The low surface roughness values indicate a non-grounded surface state, which should be related with the sub-micrometrical thickness of the splattered layers in the coating.

The data shown in Table 3 revealed an inverse relation between  $\text{TiO}_2$  composition (wt%) and coating thickness, with an increase in the amount of  $\text{TiO}_2$  added to the coating resulting in a reduced coating thickness. This effect of  $\text{TiO}_2$  composition on the coating is likely related to the lower melting point and specific heat of  $\text{TiO}_2$  in comparison to  $\text{Al}_2\text{O}_3$  [15, 19, 24]. It is known that an increment in  $\text{TiO}_2$  content produces better melted layers, resulting in a thinner coating; in contrast, with increasing  $\text{Al}_2\text{O}_3$  content the percentage of the unmelted structure increases. The  $\text{TiO}_2$  content acts as a bonding layer wrapping  $\text{Al}_2\text{O}_3$  particles, covering them during the melting process and providing an additional source of heat. A more detailed description of this process is given by Bannier et al. [25].

Data on samples produced by APS from the studies of Pawlowski et al. [9] and Xiao et al. [10] were compared with our samples produced by SPS. Compared to the APS samples, our SPS samples had a reduced coating thickness. A direct relation between coating thickness, solid particle mass ratio and feedstock size particle was evident in our SPS samples, which is consistent with the observations of Fauchais et al. [24].

Micrographs from SEM with back-scattered electrons (BSE) (Fig. 2) show the element distribution for the microstructure of the alumina–titania coatings. In general, microstructure observations revealed a layer with splat morphology in the deposits. Contrast obtained by the BSE

**Fig. 1** Scanning electron microscopy (SEM) micrographs of cross-sections of the alumina and alumina (A)–titania (T) coatings: **a** AT, **b** AT13, **c** AT25, **d** AT40. See footnote to Table 1 for definition of AT

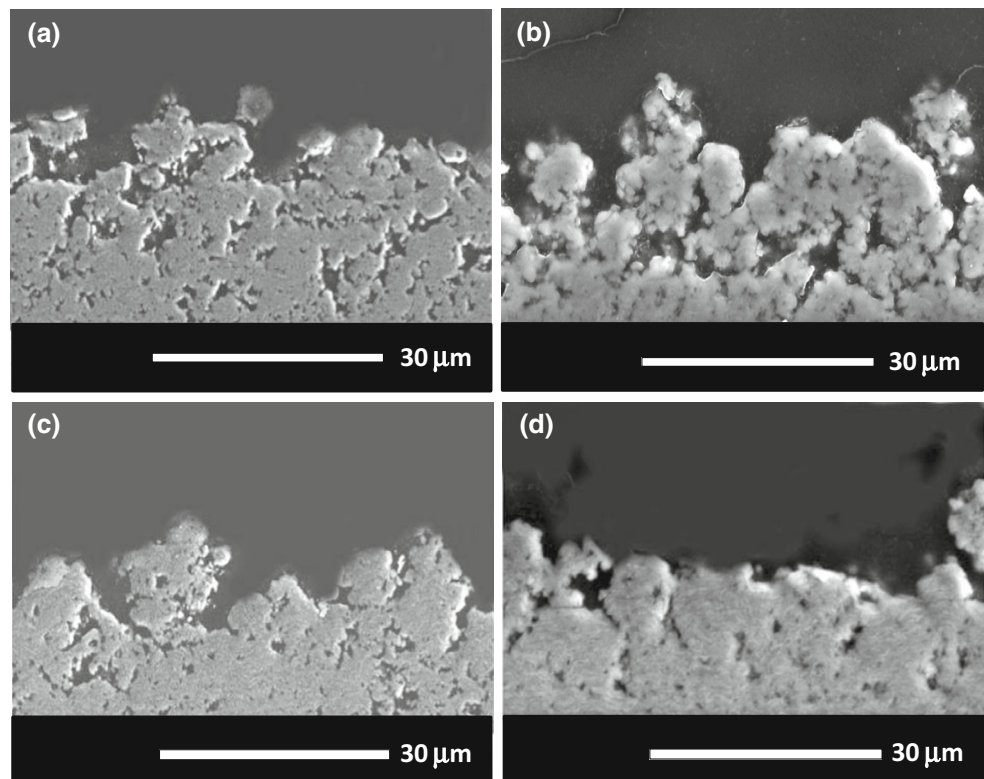


**Table 3** Thickness and roughness of alumina and alumina–titania coatings

Thickness/roughness	AT coatings			
	AT	AT13	AT25	AT40
Thickness ( $\mu\text{m}$ )	$21.1 \pm 0.8$	$16.3 \pm 9.3$	$16.6 \pm 4.9$	$15.9 \pm 1.8$
$R_a$ initial ( $\mu\text{m}$ )	3.84	4.35	3.12	3.25
$R_a$ final ( $\mu\text{m}$ )	1.96	1.31	1.052	0.706

$R_a$  Surface roughness measurement

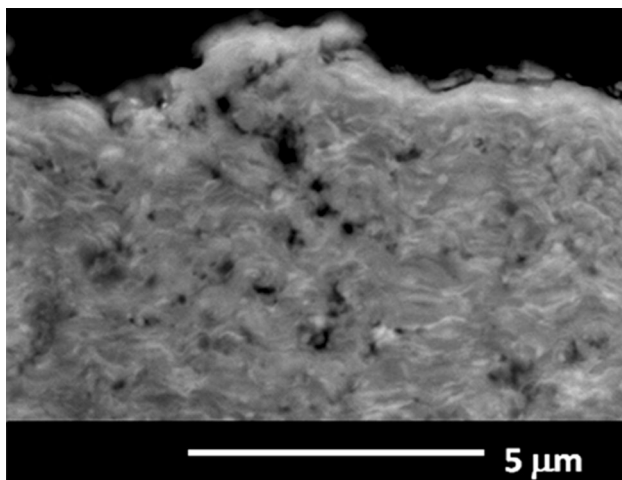


**Fig. 2** SEM with back-scattered electrons micrograph of a cross-section of the AT40 coating

technique suggests that dark particles represent areas rich in aluminum while light-gray layers are indicative of heavier elements, such as titanium. Cracks in coating microstructure (intra-lamellar failures) and delamination (inter-lamellar failures) were not found at this image resolution. Cohesion between splats was good. For more details on the interlamellar zone and coating cohesion, the reader is referred to the study of Darut et al. [26].

Content of the coatings at different phases was measured, and no evaporation of  $\text{TiO}_2$  was observed. According to the EDX/SEM data, the ratios of the elements present in the obtained coatings correspond to their respective proportions in the initial feed stock composition (Table 4).

As shown in Fig. 2, the SPS coating samples exhibited a finer microstructure than the APS samples. The thickness of the splat layers in the SPS coating samples was

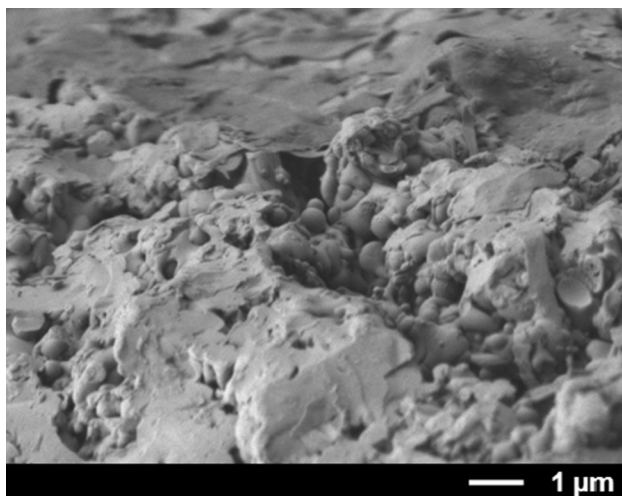


**Table 4** Proportions of the elements in deposits, calculated semi-quantitatively calculated in the energy dispersive X-ray analysis

Reference values	AT coatings		
	AT13	AT25	AT40
% Al <sub>2</sub> O <sub>3</sub>	85.93	70.56	37.12
% TiO <sub>2</sub>	14.13	29.44	62.48

<100 nm. In this case, projection with the SPS technique produced splats on the same scale as the initial feedstock size (300–400 nm).

Nanostructured materials (called also nanophased) are defined by Pawlowski et al. [9] as materials with a crystal grain size of <100 nm. Very small crystals should contain fewer than tens of thousands of atoms. The microstructure of thermal coatings [27] consists of three types of particles that are related to the different trajectories of the plasma jet and the amount of heat exposure, namely: (1) untreated particles with a grain size in the range of the initial feedstock, as well as poorly treated particles which travel in the fringes of the plasma jet and remain embedded in the coating during deposition; (2) well-melted particles which form splats in the microstructure of the coating; (3) re-solidified particles, i.e. spherical particles with a grain size of <100 nm. The last two types of particles travel in the core of the plasma, i.e. the hottest region. Figure 3 shows the fracture of a coating that presents some sort of “cauliflower” feature with well-melted grains (spherical shape) and a few unmelted ones. This example is not that of a nanometric coating, but of a nanostructured coating

**Fig. 3** Field emission SEM micrograph of the fracture surface in an AT coating

with a few elements of the structure in the nanometric size range.

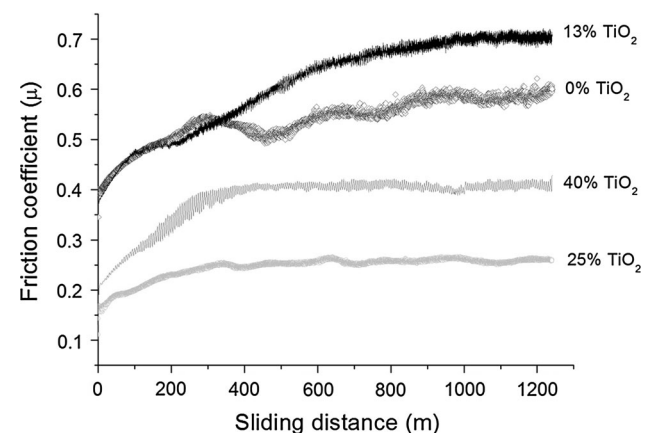
Fracture morphology of the SPS coatings was observed on FESEM micrographs. The architecture of the microstructure of an alumina (A)–titania (T) (Al<sub>2</sub>O<sub>3</sub>–TiO<sub>2</sub>) (AT) coating throughout the fracture is shown in Fig. 3 and included well-molten particles that formed flattened lamellae, unmelted particles from the initial feedstock and molten particles that were smaller than the initial feedstock. The latter had had sufficient time to re-solidify but did not reach the required speed to flatten against the substrate. This structure has also been found by other investigators [12, 28, 29].

Finally, SPS coatings showed the same size scale as the initial scale feedstock (submicrometer) and a reduction in the scale size of some particles to the near-nanometric range. This improvement in coating microstructure was related to the accurate spraying conditions selected for the SPS process, which achieved a perfectly solidified coating. The near-nanometric structure is one of the most important characteristics determining wear behavior in these materials, as discussed in a following section.

### 3.2 Friction Coefficient

The friction coefficient,  $\mu$ , is the ratio between the friction force and normal force. In a tribometer with a ball-on-disc configuration, friction force is continuously measured by a load cell with a piezoelectric transducer positioned over the loading arm. Evolution in the friction coefficient is usually separated into two different regions: running-in and steady state [19]. The first stage is related to the running of materials against themselves, while in the second stage it is assumed that both part and counterpart form a system [30].

The evolution of the friction coefficient as a function of sliding distance is reported in Fig. 4 for all tested materials. In general, first observations indicated that the addition of

**Fig. 4** Evolution of the friction coefficient with sliding distance for the studied AT coatings

TiO<sub>2</sub> to the coatings reduced the friction coefficient, except in the case of coating AT13. Moreover, regular friction coefficient behavior was observed in materials containing TiO<sub>2</sub>, while this behavior became irregular in the AT coating.

We classified the behavior of the friction coefficients of the evaluated AT coatings into two groups for a better understanding of the friction phenomenon involved, with AT and AT13 in one group and AT25 and AT40 in the other group.

In the first group, the running-in state was extended in material without TiO<sub>2</sub> (sliding distance of up to 900 m), while the inclusion of 13 %TiO<sub>2</sub> reduced this effect (sliding distance up to 700 m). Although both coatings showed an increase in the friction coefficient, the evolution was irregular in AT. This latter behavior is determined by an abrupt removal of fragments from the material, which constitutes the tribopair, producing an increase in plowing and a third body in the contact zone [31]. Irregularities found in the AT material can be attributed to a larger contribution of the third body which remained and circulated in the contact area. With continued sliding, the steady state is reached in both materials, up to 1200 m of sliding distance. This behavior can be justified with the multi-asperity contacts theory of Zhang et al. [32, 33] which suggests that friction coefficient evolution is due to three components: adhesion, asperity plowing and debris plowing.

Materials in the second group showed a similar friction behavior that is characterized by a reduction of the extension of the running-in state of up to 400 m of sliding distance in comparison with the first group. This behavior can be attributed to asperities in the plowing effect of hard coatings to soft counter material surfaces and a small contribution of wear debris. With continued sliding, the steady state is reached in both materials and maintained until the end of the test with a constant friction coefficient. Friction behavior in these materials is dominated by asperity polishing and a reduction in the generation of wear debris.

It should be noted here that although some studies have provided information on friction coefficient values in Al<sub>2</sub>O<sub>3</sub> and Al<sub>2</sub>O<sub>3</sub>-13TiO<sub>2</sub> APS coatings [17, 19, 30, 34], insufficient data remain available on Al<sub>2</sub>O<sub>3</sub>-25TiO<sub>2</sub> and Al<sub>2</sub>O<sub>3</sub>-40TiO<sub>2</sub> coatings [17, 35].

In our study, the addition of TiO<sub>2</sub> reduced the friction coefficient value in all coatings tested, with the exception of the AT13 combination. However, the value of the friction coefficient of AT13 is lower than those reported by Guesama et al. [30] and Bolelli et al. [34] for micrometric coatings. Material AT25 showed the lowest friction coefficient for AT material, namely a reduction of 62 %. It should be noted that this friction coefficient value is lower than the values reported by Dejang et al. [17] and Fervel et al. [19] for sub-micrometric and nanostructure coatings.

**Table 5** Wear scar dimensions of evaluated coatings

Coating	Width (mm)	Depth (μm)	$V_{wear}$ (mm <sup>3</sup> )
AT	0.42	15	1.65
AT13	0.40	11.1	1.11
AT25	0.38	9.3	0.87
AT40	0.28	9.2	0.66

$V_{wear}$  Wear volume loss

### 3.3 Wear Characteristic

Wear resistance is not a material property, and wear mechanisms and the associated volumetric wear rate,  $K_v$ , depend critically on the specific conditions to which they are subjected [36]. Wear scar dimensions of evaluated coatings after the test are presented in Table 5. As can be seen, no true differences were observed in the real contact area in the material surface. The lowest values of penetration depth were recorded for the coating with the most TiO<sub>2</sub> content, AT40.

Figure 5 shows the wear rate results as a function of TiO<sub>2</sub> composition for all tested materials. First observations indicated an inverse relation between wear rate and TiO<sub>2</sub> composition, with wear rates decreasing (wt%) with increasing TiO<sub>2</sub> content. This behavior is consistent with results reported by Fervel et al. [19], Bolelli et al. [34] and Ahn et al. [37].

The excellent response in wear resistance resulting from the addition of TiO<sub>2</sub> can be attributed to the effect of titania in improving the binding of sprayed alumina particles in the coating, which results in the reduction of wear of particles or lamellae in the coating [15]. Indeed, an increase in TiO<sub>2</sub> composition as small as 13 % (AT13) enabled an 1.5-fold increase in wear resistance compared with material without TiO<sub>2</sub> (AT).

The best response to dry sliding wear resistance was shown by material AT40, with a 2.6-fold increase in wear resistance compared to the AT coating material. Several authors [16, 38, 39] have proposed that the wear of brittle ceramics is proportional to fracture toughness on the basis that wear occurs by brittle cracking. Increases in the amount of TiO<sub>2</sub> added to the coating results in the formation of a denser splat layer, which in turn allows an increase in fracture toughness and a subsequent increase in wear resistance.

### 3.4 Wear Surface Observation

Wear is an extremely complex process that is affected by many factors. In certain cases, one or more factors will dominate the wear resistance of the materials, but these can and will change as conditions change [3]. Several wear

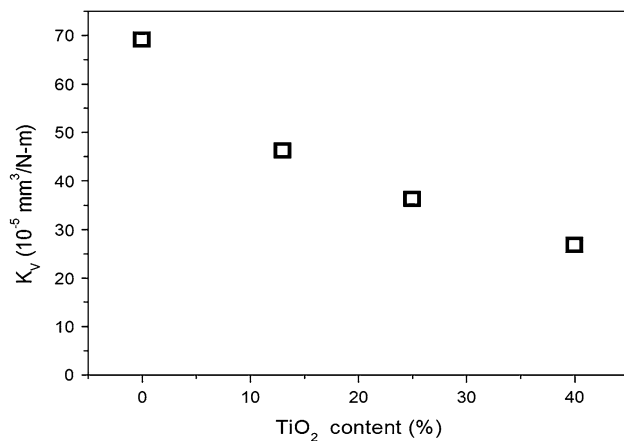


**Fig. 5** Wear rate as a function of TiO<sub>2</sub> content of the tested coatings

mechanisms, such as abrasion, adhesion, micro-fractures and delamination (separated or combined), contribute to the wear damage in ceramic–ceramic sliding contact [40].

SEM micrographs of wear tracks are shown in Fig. 6. Different levels of surface damage were observed. The observed patterns of wear damage were consistent with the wear rate behaviors presented by coating samples. Thus, material to which no TiO<sub>2</sub> had been added, AT, shows the worst damage, while AT13 and AT25 are in a previously

damaged state and AT40 shows almost no wear signs on the surface.

The very poor pattern of damage observed in the AT material (Fig. 6a) is due to the coexistence of several wear mechanisms. The wear track in Fig. 6a has the appearance of a compact wear debris layer adhering to the surface. The splats of the Al<sub>2</sub>O<sub>3</sub> coatings are detached by brittle fracture [20, 41], and debris is found in the subsequent fragmentation of these splats. Wear debris is embedded or pulled out of the wear track, creating a tribological layer, with the abrasion mechanism acting on the tribolayer at the same time that the brittle fracture appears. The debris, which remains in the contact surface, constitutes a “third body” in the sliding system and influences the contact stresses and wear [42]. In addition, grooving, microfracture and some holes are observed in the tribolayer [43] due to removal of particles as a product of the wear process.

The improvement in wear resistance of material AT13 in comparison with material AT is supported by the wear damage patterns (Fig. 6b). The wear track of material AT13 shows an irregular tribolayer, with areas where splats were plastically deformed and other areas where wear debris is attached. Wear debris is removed from the surface due to the abrasion wear mechanism, although to a lesser degree than in material AT due to the best bonding strength

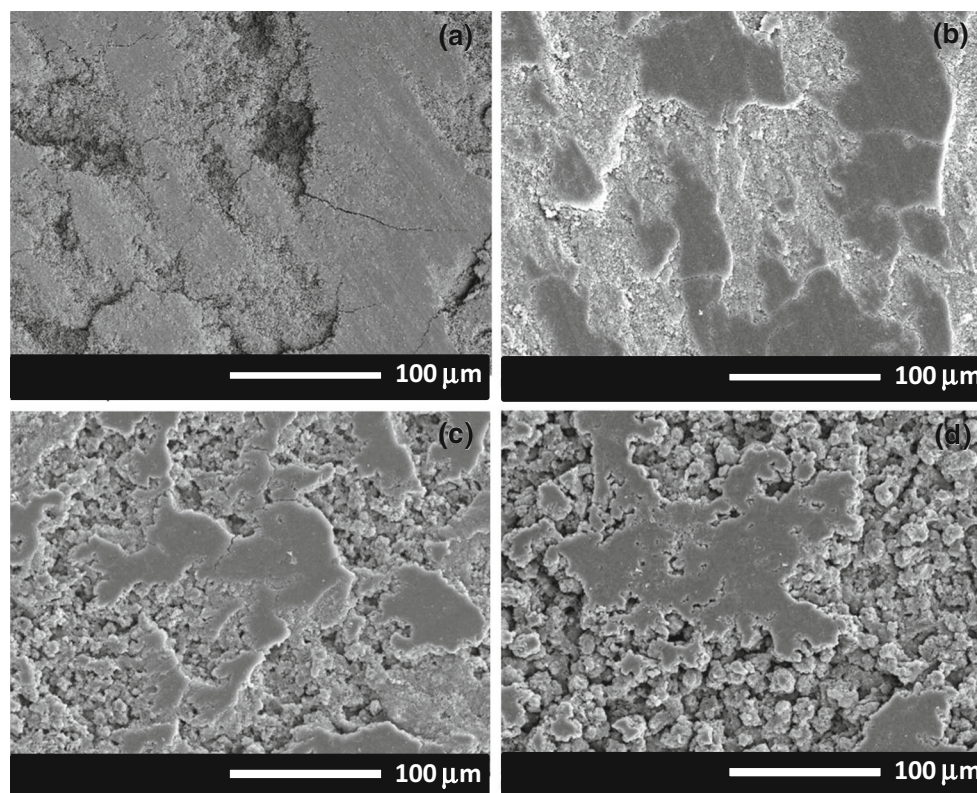


**Fig. 6** SEM micrographs of wear tracks of the tested coatings: **a** AT, **b** AT13, **c** AT25 and **d** AT40



between splats in this coating. As movement continues, the adhesion wear mechanism appears, and wear debris adheres to the surface, where it accumulates in holes and abrasion grooves to finally create the tribolayer. In addition, several cracks perpendicular to the sliding movement were observed, and these are propagated through deformed areas [11]. Hence, the presence of TiO<sub>2</sub> in the coating increases fracture toughness and reduces the strain hardening component.

Dry sliding wear resistance was remarkably improved in materials AT25 (Fig. 6c) and AT40 (Fig. 6d). Observation of the wear tracks indicates a damage stage prior to that of material AT13, which is in accordance with our data on the wear rates. However, material AT25 shows a worse pattern of pattern damage than material AT40. The wear track in material AT25 shows asperity deformation, plowing in the sliding direction, a few holes due to particles being removed and plastically deformed splats. There is no evidence of a consistent tribolayer, although the formation of wear debris is observed in the damage surface. The wear track of material AT40 shows a small presence of plastically deformed splats and an incipient abrasion mechanism that is evidence of the excellent wear resistance of this material.

Near-nanometric structures obtained by SPS in these coatings lead to splats, melting particles, partial melting particles and defects that involve the microstructure remaining in the same size range. Furthermore, an increase in inter-lamellar cohesion and wear resistance is directly linked to a reduction in defect sizes. The addition of TiO<sub>2</sub> to the coatings improved structure densification and ductility, which in turn enhanced dry sliding wear resistance. The extraction of particles from wear surfaces becomes more difficult with an increasingly dense microstructure, and an increase in ductility produces more plastic flow, which inhibits the appearance of wear debris. Ultimately, the greatest improvement in the dry sliding wear resistance of these coatings is achieved by the combination of near-nanometric structure and the addition of TiO<sub>2</sub>.

## 4 Conclusions

The friction and wear behavior of alumina and alumina–titania coatings fabricated by SPS was studied in a ball-on-disk tribometer. The following observations were made:

- The microstructure of coatings obtained by SPS were on the same size scale as that of the initial feedstock, presenting at the same time some particles in which the microstructure was reduced to near-nanometric scale. The accurate definition of spraying conditions played an important role in the final result.
- A noticeable reduction in friction coefficient was found in coatings with the addition of more than 13 wt% titania. An important reduction of 62 % in the friction coefficient value was found in coatings with 25 wt% titania.
- The wear rate was inversely affected by the wt% of TiO<sub>2</sub> in the coatings. The addition of 40 wt% titania increased dry sliding wear resistance by 2.6-fold compared to that of the 100 wt% alumina coating.
- The improved sliding wear resistance of coatings can be attributed to the combination of the addition of titania and the near-nanometric structure obtained by SPS. The former provided a better structure densification and ductility, while the reduction in grain size reduced the number of defects, splats and melting particles.
- The marked differences found in the wear resistance coatings tested were corroborated by the damage patterns observed in the wear tracks. The wear mechanism is controlled by plastic deformation, asperity deformation, abrasion in the sliding movement, pulled-out particles and tribolayer formation.

**Acknowledgments** The authors wish to thank for the Spanish Ministry of Economy and Competitiveness (MAT2012-38364-C03) and the Autonomous Government of Valencia for funding for the stay in SPCTS-UMR CNRS (France), and the French FCENANOSURF consortium funded by the French Ministry and Industry and local governments of Région Centre and Région Limousin.

## References

1. Pawlowski, L.: *The Science and Engineering of Thermal Spray Coatings*. Wiley: Hoboken (2008)
2. Lampe, Th, Eisenberg, S., Cabeo, E.R.: Plasma surface engineering in the automotive industry—trends and future prospective. *Surf. Coat. Technol.* **174–175**, 1–7 (2003)
3. Wang, Y., Jiang, S., Wang, M., Wang, S., Xiao, T.D., Strutt, P.R.: Abrasive wear characteristics of plasma sprayed nanostructured alumina/titania coatings. *Wear* **237**, 176–185 (2000)
4. Kabacoff, L.T.: Nanoceramic coatings exhibit much higher toughness and wear resistance than conventional coatings. *AMPITAC Newslett.* **6**(1), 37–42 (2002)
5. Wang, M., Shaw, L.L.: Effects of the powder manufacturing method on microstructure and wear performance of plasma sprayed alumina–titania coatings. *Surf. Coat. Technol.* **202**, 34–44 (2007)
6. Shaw, L.L., Goberman, D., Ren, R., Gell, M., Jing, S., Wang, Y., Xiao, T.D., Strutt, P.R.: The dependency of microstructure and properties of nanostructured coatings on plasma spray conditions. *Surf. Coat. Technol.* **130**, 1–8 (2000)
7. Dahotre, N.B., Nayak, S.: Nanocoatings for engine application. *Surf. Coat. Technol.* **194**(1), 58–67 (2005)
8. Sathish, S., Geetha, M., Aruna, S.T., Balaji, N., Rajam, K.S., Asokamani, R.: Sliding wear behavior of plasma sprayed nanoceramic coatings for biomedical applications. *Wear* **271**, 934–941 (2011)



9. Pawlowski, L.: Finely grained nanometric and submicrometric coatings by thermal spraying: a review. *Surf. Coat. Technol.* **202**, 4318–4328 (2008)
10. Xiao, D., Wang, Y., Strutt, P.: Fabrication and evaluation of plasma sprayed nanostructured alumina–titania coatings with superior properties. *Mater. Sci. Eng.* **301**, 80–89 (2001)
11. Tjong, S.C., Chen, H.: Nanocrystalline materials and coatings. *Mater. Sci. Eng.* **45**, 1–88 (2004)
12. Fauchais, P., Montavon, G., Bertrand, G.: From powders to thermally sprayed coatings. *J. Therm. Spray Technol.* **19**, 56–80 (2010)
13. Lima, R.S., Marple, B.R.: Thermal spray coatings engineered from nanostructured ceramic agglomerated powders for structural, thermal barrier and biomedical applications: a review. *J. Therm. Spray Technol.* **16**, 40–63 (2007)
14. Fauchais, P., Etchart-Salas, R., Delbos, C., Tognonvi, M., Rat, V., Coudert, J.F., Chartier, T.: Suspension and solution plasma spraying of finely structured layers: potential application to SOFCs. *J. Phys. D Appl. Phys.* **40**, 2394–2406 (2007)
15. Ramachandran, K., Selvajaran, V., Ananthapadmanabhan, P.V., Sreekumar, K.P.: Microstructure, adhesion, micro hardness, abrasive wear resistance and electrical resistivity of the plasma sprayed alumina and alumina–titania coatings. *Thin Solid Films* **315**, 144–152 (1998)
16. Lee, S.W., Morillo, C., Lira-Olivares, J., Kim, S.H., Sekino, T., Niihara, K., Hockey, B.J.: Tribological and microstructural analysis of Al<sub>2</sub>O<sub>3</sub>/13TiO<sub>2</sub> nanocomposites to use in femoral head of hip replacement. *Wear* **225**, 1040–1044 (2003)
17. Dejang, N., Watcharapasorn, A., Wirojupatump, S., Niranatlumpong, P., Jiansirisomboon, S.: Fabrication and properties of plasma-sprayed Al<sub>2</sub>O<sub>3</sub>/TiO<sub>2</sub> composite coatings: a role of nano-sized TiO<sub>2</sub> addition. *Surf. Coat. Technol.* **204**, 1651–1657 (2010)
18. Yimaz, S.: An evaluation of plasma sprayed coatings based on Al<sub>2</sub>O<sub>3</sub> and Al<sub>2</sub>O<sub>3</sub>–13wt% TiO<sub>2</sub> with bond coat on pure titanium substrate. *Ceram. Int.* **35**, 2017–2022 (2009)
19. Fervel, V., Normand, B., Coddet, C.: Tribological behavior of plasma sprayed Al<sub>2</sub>O<sub>3</sub>-based cermet coatings. *Wear* **230**(1), 70–77 (1999)
20. Vargas, F., Ageorges, H., Fauchais, P., López, M.E.: Mechanical and a tribological performance of Al<sub>2</sub>O<sub>3</sub> coatings elaborated by flame and plasma spraying. *Surf. Coat. Technol.* **205**, 1132–1136 (2010)
21. Bacciocchini, A., Ilavsky, J., Montavon, G., Denoirjean, A., Benettouil, F., Valette, S., Fauchais, P., Wittmann-teneze, K.: Quantification of void network architectures of suspension plasma-sprayed (SPS) yttria-stabilized zirconia (YSZ) coatings using ultra-small-angle X-ray scattering (USAXS). *Mater. Sci. Eng.* **528**, 91–102 (2010)
22. ASTM International: ASTM G99-03: Standard test method for wear testing with a pin-on-disc apparatus. ASTM annual book of standards. ASTM International: West Conshohocken (2003)
23. Lancaster, K.: The influence of substrate hardness on the formation and endurance of molybdenum disulphide films. *Wear* **10**, 103–107 (1967)
24. Fauchais, P., Rat, V., Delbos, C., Fazilleau, J., Coudert, J.F., Chartier, T., Bianchi, L.: Understanding of suspension plasma spraying of finely structured coatings for SOFC. *IEEE Plasma Sci.* **33**(2), 920–930 (2005)
25. Bannier, E., Vicent, M., Rayón, E., Benavente, R., Salvador, M.D., Sánchez, E.: Effect of TiO<sub>2</sub> addition on the microstructure and nanomechanical properties of Al<sub>2</sub>O<sub>3</sub> suspension plasma sprayed coatings. *Appl. Surf. Sci.* **316**, 141–146 (2014)
26. Darut, G., Klyatskina, E., Valette, S., Carles, P., Denoirjean, A., Montavon, G., Ageorges, H., Segovia, F., Salvador, M.D.: Architecture and phases composition of suspension plasma sprayed alumina–titania sub-micrometer-sized coatings. *Mater. Lett.* **67**, 241–244 (2012)
27. Fauchais, P., Montavon, G.: Latest developments in suspension and liquid precursor thermal spraying. *J. Therm. Spray Technol.* **19**(1–2), 226–239 (2010)
28. Darut, G., Ben-Ettouli, F., Denoirjean, A., Montavon, G., Ageorges, H., Fauchais, P.: Dry sliding behavior of sub-micrometer-sized suspension plasma sprayed ceramic oxide coatings. *J. Therm. Spray Technol.* **19**, 275–285 (2010)
29. Tingaud, O., Bacciocchini, A., Montavon, G., Denoirjean, A., Fauchais, P.: Suspension DC plasma spraying of thick finely-structured ceramic coatings: process manufacturing mechanisms. *Surf. Coat. Technol.* **203**, 2157–2161 (2009)
30. Guesama, S., Bounazef, M., Nardin, P., Sahraoui, T.: Wear behavior of alumina–titania coatings: analysis of process and parameters. *Ceram. Int.* **32**, 13–19 (2006)
31. Espinosa-Fernández, L., Borrell, A., Salvador, M.D., Gutierrez-Gonzalez, C.F.: Sliding wear behavior of WC–Co–Cr<sub>3</sub>C<sub>2</sub>–VC composites fabricated by conventional and non-conventional techniques. *Wear* **307**, 60–67 (2013)
32. Zhang, J., Moslehy, F.A., Rice, S.L.: A model for friction in quasi-steady-state. Part I. Derivation. *Wear* **149**, 1–12 (1991)
33. Zhang, J., Moslehy, F.A., Rice, S.L.: A model for friction in quasi-steady-state sliding Part II. Numerical results and discussion. *Wear* **149**, 13–25 (1991)
34. Bolelli, G., Cannilo, V., Lusvardi, L., Manfredini, T.: Wear behaviour of thermally sprayed ceramic oxide coatings. *Wear* **261**, 1298–1315 (2006)
35. Normand, B., Fervel, V., Coddet, C., Nikitine, V.: Tribological properties of plasma sprayed alumina–titania coatings: next term role and control of the microstructure. *Surf. Coat. Technol.* **123**, 278–287 (2000)
36. Hutchings, I.: Tribology: friction and wear of engineering materials. *Mater. Des.* **13**, 187 (1992)
37. Ahn, J., Hwang, B., Song, E.P., Lee, S., Kim, N.J.: Correlation of microstructure and wear resistance of Al<sub>2</sub>O<sub>3</sub>–TiO<sub>2</sub> coatings plasma sprayed with nanopowders. *Metall. Mater. Trans. A* **37**, 1851–1860 (2006)
38. Erickson, L.C., Hawthorne, H.M., Troczynski, T.: Correlations between microstructural parameters, micromechanical properties and wear resistance of plasma sprayed ceramic coatings. *Wear* **250**, 569–575 (2001)
39. Song, E.P., Ahn, J., Lee, S., Kim, N.J.: Microstructure and wear resistance of nanostructured Al<sub>2</sub>O<sub>3</sub>–8 wt%TiO<sub>2</sub> coatings plasma-sprayed with nanopowders. *Surf. Coat. Technol.* **201**, 1309–1315 (2006)
40. Tucker Jr., R.C.: ASM Handbook Volume 5A: Thermal Spray Technology. ASM International, Materials Park (2013)
41. Stachowiack, G.W., Batchelor, A.: Engineering Tribology Handbook. Elsevier-Butterworth-Heinemann: Oxford (2005)
42. Fischer, T.E., Zhu, Z., Kim, H., Shin, D.S.: Genesis and role of wear debris in sliding wear of ceramics. *Wear* **245**, 53–60 (2000)
43. Lima, R.S., Moureau, C., Marple, B.R.: HVOF-sprayed coatings engineered from mixtures of nanostructured and submicron Al<sub>2</sub>O<sub>3</sub>–TiO<sub>2</sub> powders: an enhanced wear performance. *J. Therm. Spray Technol.* **16**, 866 (2007)